Sensor Applications

RSS-based Localization for Wireless Underground Battery-free Sensor Networks

Hongzhi Guo[1*]

[1] *Engineering Department, Norfolk State University, Norfolk, VA, 23504, USA*
[*] *Member, IEEE*

Abstract—Underground battery-free sensors do not require battery replacement which can support large-scale deployment for agriculture applications. The underground environment is dynamic, and the soil permittivity and electric conductivity vary significantly due to precipitation and irrigation. These dynamic parameters affect the accuracy of underground battery-free sensor localization. This letter proposes a localization framework using the expectation-maximization algorithm by considering the signal attenuation coefficient as a latent variable. The proposed solution is evaluated using data collected by underground sensors. Simulation results show that the root-mean-square error is around 0.3 m in various scenarios.

Index Terms—Battery-free sensors, expectation-maximization algorithm, magnetic induction communication, underground localization.

I. INTRODUCTION

Underground sensors play an important role in precision agriculture by collecting agricultural-related information in the soil, such as soil nutrition, temperature, and moisture. Wireless technologies are used to connect these sensors with the Internet of Things (IoT) gateways and servers [1], [2]. These underground sensors are powered by batteries that can operate for a long time. The recent development of wearable agriculture sensors [3] aims to use extremely thin or tiny sensors that can be attached to plants to closely monitor their growth. Usually, battery-powered sensors are bulky and heavy, and cannot support wearable agriculture sensors. Moreover, they require battery replacement and related maintenance, which are labor-intensive.

Battery-free underground sensors [4] powered by wireless signals can be designed in small sizes and lightweight that are suitable for wearable agriculture sensing. Backscatter communication is a widely used solution for battery-free sensors, where the battery-free sensor modulates and reflects incident electromagnetic waves. A ground robot or a drone can be used as a reader to excite underground battery-free sensors and collect data. However, electromagnetic wave-based wireless communication at the UHF (Ultra High Frequency) band is not suitable for densely deployed wearable agriculture sensors. First, UHF signals have a long communication range in the air, which creates interference and competes for spectrum with existing applications. Also, UHF signal propagation is significantly affected by the soil medium due to reflection and attenuation. Most agricultural activities are in the shallow underground environment with a depth smaller than 0.5 m. Thus, on one hand, the wireless communication technology that is used for underground battery-free sensors must have a communication range longer than 0.5 m. On the other hand, the communication range should be kept as small as possible to reduce the interference to nearby wireless applications. Moreover, it should be efficient in penetrating the soil. Magnetic induction communication (MIC) uses the near field of RF signals to efficiently penetrate inhomogeneous soil medium, and the magnetic fields in the near field fall off fast, which creates negligible interference [5].

As shown in Fig. 1, a ground robot is used to communicate with underground battery-free sensors using MIC [4]. A large number of these sensors can be deployed densely around a plant – both underground and aboveground. First, the robot broadcasts magnetic fields, and the underground battery-free sensor harvests energy. Then, the sensor performs sensing and uses load-modulation to send back data. The robot can receive load-modulated data using the same coil or a different coil that is dedicated to receiving [6]. Localization of underground sensors is essential to better leverage the sensing data for agriculture applications.

Localizing underground battery-free sensors faces the following challenges. First, although MIC has a stable wireless channel in inhomogeneous media compared with far-field electromagnetic wave-based wireless communication, the soil conductivity and permittivity dynamics still affect the MIC channel, particularly the attenuation coefficient. Second, anchor nodes are not always available due to the limited communication range and the densely deployed sensors. Existing underground MIC localization algorithms use anchor nodes and do not consider the dynamic environment. This can be used for active underground MIC sensors, as shown in Fig. 1, which have a longer communication range and anchors are available. For the dense deployment considered in this letter, the active underground MIC sensors are not optimal. This letter considers the soil dynamics for load-modulated MIC. First, by showing the collected data using underground sensors in the Thoreau system [7], [8], we show that the attenuation coefficient is also dynamic. Then, we develop an expectation-maximization (EM) algorithm to localize underground battery-free sensors by considering the attenuation coefficient as a latent variable. We only use the received signal strength (RSS) since it is widely available in wireless radios. The proposed solution is numerically evaluated and compared in different scenarios.

II. DYNAMIC CHANNEL

As shown in Fig. 1, the robot first broadcasts magnetic fields towards underground battery-free sensors. These sensors first harvest energy and perform sensing. Then, they use load-modulation to send data back to the robot. In this letter, we consider the transmitter and the receiver on the robot to use separated coils for better signal detection [6]. The signal transmission is based on coil coupling. The mutual coupling between the transmitter and the receiver on the robot is neglected. This can be addressed using self-interference cancellation techniques in practice.

1) Channel Model: For point-to-point MIC with only the forward path, the received power is $P_r = l_f P_t$, where $l_f \sim (\omega M)^2$ is the

Corresponding author: H. Guo (e-mail: hguo@nsu.edu)
This work was supported by National Science Foundation under grant no. CNS1947748.

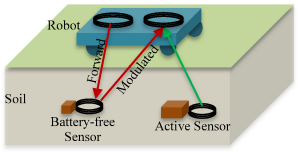

Fig. 1: Load-modulation MIC and active MIC.

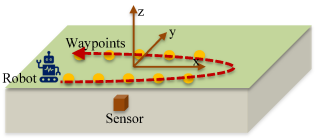

Fig. 2: Robot trajectory for RSS signal collection.

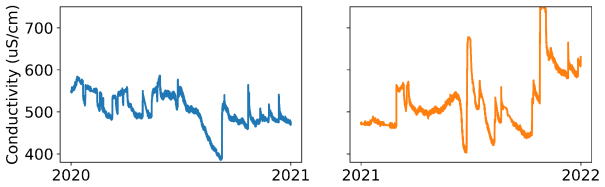

Fig. 3: Electric conductivity of the soil measured by an underground sensor in 2020 and 2021.

linear forward path loss, P_t is the transmission power, $\omega = 2\pi f_c$, f_c is the signal carrier frequency, and M is the mutual inductance between the transmit coil and the receive coil [5]. For load-modulation MIC, the transmitter and the receiver are almost in the same location and their coil configurations are the same. The backward path loss can be approximated by the forward path loss l_f. The load-modulated signal has a slight frequency shift compared with the incident signal. However, this frequency shift is negligible compared with the carrier frequency. Thus, the received signal strength of load-modulation MIC is proportional to $(\omega M)^4 P_t$.

The soil has a certain conductivity, and wireless signals attenuates as they propagate in the soil. The mutual inductance considering soil conductivity can be approximated by $M \approx \frac{C_m}{d^3} e^{-\alpha d}$, where C_m is a constant which is determined by coil configurations, d is the distance between the robot and the sensor, and $\alpha = \omega\sqrt{\frac{\varepsilon\mu}{2}}\left[\sqrt{1+\left(\frac{\sigma}{\omega\varepsilon}\right)^2}-1\right]^{1/2}$. The soil permeability, permittivity, and conductivity are represented by μ, ϵ, and σ, respectively. The misalignment between the coils in the robot and sensor is not considered. Existing research has shown that the misalignment loss can be addressed by using coil arrays on the robot [4]. As a result, the RSS of load-modulation MIC in dB scale is $P_r \approx C_p - 17.4\alpha d - 120\log_{10} d + n$, where $C_p = 10\log_{10} P_t + 40\log_{10}(\omega C_m)$ and n is the noise due to RSS receiving and measurement which subjects to the Guassian distribution, i.e., $n \in \mathcal{N}(0, \sigma_n^2)$.

2) Dynamic Attenuation Coefficient: The soil conductivity is related to the volumetric water content, which is a dynamic parameter that is affected by precipitation and irrigation. In this paper, we use the data collected through the Thoreau platform [7], [8]. An example of the conductivity is shown in Fig. 3. While not shown here, the permittivity has a similar pattern. The data was measured by an underground sensor in 2020 and 2021. As we can see, conductivity is a dynamic parameter that vary significantly during a year. Due to different weather conditions, there is an obvious difference between the two years. The conductivity and permittivity can be different at different depths. We consider the soil is homogeneous with the same conductivity and permittivity at any depths. The associated attenuation coefficient at 13.56 MHz is shown in Fig. 4. This frequency is used since it is an ISM frequency band and battery-free sensors using Near Field Communication (NFC) protocols are available. MIC uses lower MHz band signals to increase the wavelength and reduce the attenuation losses. Thus, the attenuation coefficient is stable with small values.

To capture this dynamic process, the attenuation coefficient at time

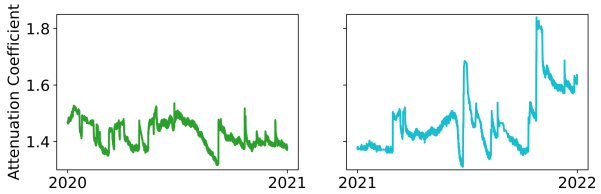

Fig. 4: Attenuation coefficient of soil.

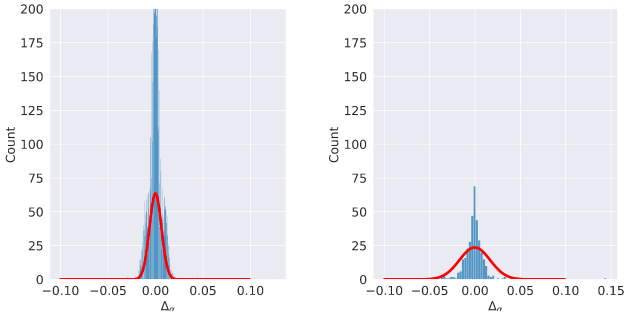

(a) Hourly resampled Δ_α. Approximated by a Gaussian distribution with mean 0 and standard deviation 0.0063.

(b) Daily resampled Δ_α. Approximated by a Gaussian distribution with mean 0 and standard deviation 0.0169.

Fig. 5: Distribution of Δ_α using the attenuation coefficient in 2020.

step t can be considered as $\alpha^t = \alpha^{t-1} + \Delta_\alpha$, where Δ_α is a Gaussian random variable with mean m_α and standard deviation δ_α, and α^{t-1} is the attenuation coefficient at time step $t-1$. The distribution of Δ_α is shown in Fig. 5. Since the original data was sampled at different time intervals due to data missing and node failures, we resampled the data and make the sampling interval as a constant. In Fig. 5a, the time interval for one step is one hour, while in Fig. 5b, it is one day. As shown in Fig. 5b, the distribution of both the hourly and daily sampled Δ_α can be approximated by Gaussian. The daily change is more significant and it demonstrates a large standard deviation compared to the hourly change.

III. EXPECTATION-MAXIMIZATION LOCALIZATION

The EM algorithm [9] is an iterative solution with the expectation and maximization steps to estimate unknown parameters with partial observations. In this paper, the received power $\boldsymbol{r}$ and aboveground robot trajectory $\boldsymbol{X}_r = [\boldsymbol{x}_1, \boldsymbol{x}_2, \cdots, \boldsymbol{x}_N]$ are known, while the underground battery-free sensor location $\boldsymbol{x}_0$ and attenuation coefficient $\alpha(t)$ are unknown. The objective is to estimate $\boldsymbol{x}_0$ with the latent variable α^t which is determined by the soil states. Considering the unknown attenuation coefficient, the problem is

$$\tilde{\boldsymbol{x}}_0 = \arg\max_{\boldsymbol{x}_0} \int p(\boldsymbol{x}_0, \alpha^t | \boldsymbol{r}, \boldsymbol{X}_r) d\alpha^t. \tag{1}$$

The probability $p(\boldsymbol{x}_0, \alpha^t, \boldsymbol{r}, \boldsymbol{X}_r)$ has a simple analytical expression. The EM algorithm first generates α^t based on observed $\boldsymbol{r}$ and $\boldsymbol{X}_r$, and an initial estimation of the sensor location $\tilde{\boldsymbol{x}}_0^k$, where k represents the iteration number. This is achieved by using the expectation of the logarithm of the probability $p(\boldsymbol{x}_0, \alpha^t, \boldsymbol{r}, \boldsymbol{X}_r)$. After that, $\tilde{\boldsymbol{x}}_0^{k+1}$ is obtained by maximizing the expectation expression with respect to $\boldsymbol{x}_0$. In the expectation step, we find the conditional expectation of the complete logarithm augmented density, which is

$$Q(\boldsymbol{x}_0, \tilde{\boldsymbol{x}}_0^k) = \mathbb{E}\{\log p(\boldsymbol{x}_0, \alpha^t) | \boldsymbol{r}, \boldsymbol{X}_r, \tilde{\boldsymbol{x}}_0^k\} \tag{2}$$

$$= \int p(\alpha^t | \boldsymbol{r}, \boldsymbol{X}_r, \tilde{\boldsymbol{x}}_0^k) \log p(\boldsymbol{x}_0, \alpha^t, \boldsymbol{r}, \boldsymbol{X}_r) d\alpha^t \tag{3}$$

$$= \int p(\alpha^t | \boldsymbol{r}, \boldsymbol{X}_r, \tilde{\boldsymbol{x}}_0^k) \log p(\boldsymbol{r} | \boldsymbol{x}_0, \alpha^t, \boldsymbol{X}_r) d\alpha^t$$

$$+ \log p(\boldsymbol{x}_0) + \int p(\alpha^t|\boldsymbol{r}, \boldsymbol{X}_r, \tilde{\boldsymbol{x}}_0^k) \log p(\alpha^t) d\alpha^t. \quad (4)$$

From Equ. (3) to Equ. (4), we use $p(\boldsymbol{x}_0, \alpha^t, \boldsymbol{r}, \boldsymbol{X}_r) = p(\boldsymbol{r}|\boldsymbol{x}_0, \alpha^t, \boldsymbol{X}_r) p(\boldsymbol{x}_0) p(\alpha^t)$. To find a closed-form solution, we need to find the probabilities in Equ. (4). For $p(\boldsymbol{x}_0)$, we consider the underground battery-free sensors are uniformly distributed. Thus, it can be neglected since any location has the same $p(\boldsymbol{x}_0)$. Note that, in some scenarios, $p(\boldsymbol{x}_0)$ may be considered as 3D Gaussian distributions, i.e., it has a high probability around the roots of a plant. According to the definition of α^t in Section II-2, $p(\alpha^t)$ can be written as

$$p(\alpha^t) = \frac{1}{\sqrt{2\pi}\delta_\alpha} e^{-\frac{1}{2}\left(\frac{\alpha^t - \alpha^{t-1}}{\delta_\alpha}\right)^2}. \quad (5)$$

given that α^{t-1} is known. When α^{t-1} is unknown, the distribution of α^t is still considered as Gaussian, but with different mean value and standard deviation. We will discuss the difference and the solutions to estimate $\boldsymbol{x}_0$ in these two cases.

The probability $p(\boldsymbol{r}|\boldsymbol{x}_0, \alpha^t, \boldsymbol{X}_r)$ can be written as

$$p(\boldsymbol{r}|\boldsymbol{x}_0, \alpha^t, \boldsymbol{X}_r) = \prod_{i=1}^{N} \frac{1}{(2\pi)^{\frac{1}{2}}\delta_n} e^{-\frac{1}{2}\left(\frac{\boldsymbol{r}[i] - C_p + 17.4\alpha^t \|\boldsymbol{x}_0 - \boldsymbol{x}_i\| + 120\log_{10}\|\boldsymbol{x}_0 - \boldsymbol{x}_i\|}{\delta_n}\right)^2}. \quad (6)$$

where $\boldsymbol{r}[i]$ is the received power at the i^{th} waypoint. Here, we implicitly assume that all the RSS signals are independent. The probability $p(\alpha^t|\boldsymbol{r}, \boldsymbol{X}_r, \tilde{\boldsymbol{x}}_0^k)$ can be written as $p(\alpha^t|\boldsymbol{r}, \boldsymbol{X}_r, \tilde{\boldsymbol{x}}_0^k) = p(\boldsymbol{r}|\tilde{\boldsymbol{x}}_0^k, \alpha^t, \boldsymbol{X}_r) \cdot p(\alpha^t)$, where $p(\boldsymbol{r}|\tilde{\boldsymbol{x}}_0^k, \alpha^t, \boldsymbol{X}_r)$ can be obtained by replacing $\boldsymbol{x}_0$ in Equ. (6) with $\tilde{\boldsymbol{x}}_0^k$. Since $p(\boldsymbol{r}|\tilde{\boldsymbol{x}}_0^k, \alpha^t, \boldsymbol{X}_r)$ and $p(\alpha^t)$ are Gaussian distributions, $p(\alpha^t|\boldsymbol{r}, \boldsymbol{X}_r, \tilde{\boldsymbol{x}}_0^k)$ is also proportional to a Gaussian distribution. The mean value of α^t is $u_{cd} = F_1/F_2$ and the variance is $\delta_{cd}^2 = 1/F_2$ [10], where

$$F_1 = \frac{\alpha^{t-1}}{\delta_\alpha^2} - \sum_{i=1}^{N} \frac{\boldsymbol{r}[i] - C_p + 120\log_{10}\|\tilde{\boldsymbol{x}}_0^k - \boldsymbol{x}_i\|}{17.4\|\tilde{\boldsymbol{x}}_0^k - \boldsymbol{x}_i\|(\delta_n/(17.4\|\tilde{\boldsymbol{x}}_0^k - \boldsymbol{x}_i\|))^2} \quad (7)$$

and

$$F_2 = \frac{1}{\delta_\alpha^2} + \sum_{i=1}^{N} \frac{(17.4\|\tilde{\boldsymbol{x}}_0^k - \boldsymbol{x}_i\|))^2}{\delta_n^2}. \quad (8)$$

Note that, u_{cd} and δ_{cd} are useful to derive the maximization of $Q(\boldsymbol{x}_0, \tilde{\boldsymbol{x}}_0^k)$. Since in the maximization step, we will use the derivative of $Q(\boldsymbol{x}_0, \tilde{\boldsymbol{x}}_0^k)$ with respect to $\boldsymbol{x}_0$ to find updated estimation, any item that is not related to the maximization can be removed from Equ. (4), i.e., the second and the third items can be removed and only the first item is kept.

Thus, we have an updated equation

$$Q(\boldsymbol{x}_0, \tilde{\boldsymbol{x}}_0^k) \sim \int p(\alpha^t|\boldsymbol{r}, \boldsymbol{X}_r, \tilde{\boldsymbol{x}}_0^k) \log p(\boldsymbol{r}|\boldsymbol{x}_0, \alpha^t, \boldsymbol{X}_r) d\alpha^t. \quad (9)$$

The logarithm item in the above equation can be written as a function of α^t and $(\alpha^t)^2$. The integral finds the summation of constants and the mean value and the second order moment of α^t. Finally, we obtain the following equation.

$$\begin{aligned} Q_{ap}(\boldsymbol{x}_0, \tilde{\boldsymbol{x}}_0^k) = &\sum_{i=1}^{N} 302.8(u_{cd}^2 + \delta_{cd}^2)\boldsymbol{d}[i]^2 + 14400(\log_{10}\boldsymbol{d}[i])^2 \\ &+ 4176u_{cd}\boldsymbol{d}[i]\log_{10}\boldsymbol{d}[i] + 34.8u_{cd}\boldsymbol{r}[i]\boldsymbol{d}[i] + 240\boldsymbol{r}[i]\log_{10}\boldsymbol{d}[i] \\ &- 34.8u_{cd}C_p\boldsymbol{d}[i] - 240C_p\log_{10}\boldsymbol{d}[i], \end{aligned} \quad (10)$$

where $\boldsymbol{d}[i] = \|\boldsymbol{x}_0 - \boldsymbol{x}_i\|$. Note that, $Q(\boldsymbol{x}_0, \tilde{\boldsymbol{x}}_0^k) \sim -Q_{ap}(\boldsymbol{x}_0, \tilde{\boldsymbol{x}}_0^k) + C_2$, where C_2 is a constant. Thus, maximizing $Q(\boldsymbol{x}_0, \tilde{\boldsymbol{x}}_0^k)$ in the maximization step is equivalent to minimizing $Q_{ap}(\boldsymbol{x}_0, \tilde{\boldsymbol{x}}_0^k)$. Then, by minimizing $Q_{ap}(\boldsymbol{x}_0, \tilde{\boldsymbol{x}}_0^k)$ we can obtain updated $\tilde{\boldsymbol{x}}_0^{k+1}$. This process will continue until $\|\tilde{\boldsymbol{x}}_0^{k+1} - \tilde{\boldsymbol{x}}_0^k\| < \eta$ or the predefined step number N_{step} has been reached. A summary of the EM-based localization algorithm is given in Algorithm 1. $Q_{ap}(\boldsymbol{x}_0, \tilde{\boldsymbol{x}}_0^k)$ is not linear, and it is not straightforward to obtain the solution. We use gradient decent to iteratively find the minimum value [11]. When α^{t-1} is not available, we use a general distribution of α. Consider that the soil properties can be measured monthly or even longer, e.g., soil samples are collected by robots and sent to laboratories for analysis.

Algorithm 1 Expectation-Maximization Algorithm

Input: $\boldsymbol{x}_0^1$, $\boldsymbol{X}_r$, α^{t-1}, δ_α, δ_n, C_p, N_{step}
Output: $\tilde{\boldsymbol{x}}_0$
$k = 1$.
while $k < N_{step}$ **do**
  E-step: obtain $Q_{ap}(\boldsymbol{x}_0, \tilde{\boldsymbol{x}}_0^k)$ using Equ. (10), (7), and (8).
  M-step: obtain $\tilde{\boldsymbol{x}}_0^{k+1} = \arg\min_{\boldsymbol{x}_0} Q_{ap}(\boldsymbol{x}_0, \tilde{\boldsymbol{x}}_0^k)$
  $k = k + 1$.
end while
$\tilde{\boldsymbol{x}}_0 = \tilde{\boldsymbol{x}}_0^k$.

IV. SIMULATION AND NUMERICAL ANALYSIS

A significant advantage of MIC is that it is less affected by the environment compared with the UHF electromagnetic wave communications. Thus, existing works either do not consider the impact of soil conductivity or consider the permittivity and conductivity as constants. With this in mind, our baseline model only considers the impact of distance, i.e., $M \approx C_m/d^3$. The localization problem is simplified to $\tilde{\boldsymbol{x}}_0 = \text{argmin}_{\boldsymbol{x}_0} \sum_{i=1}^{N} \left\|\boldsymbol{r}[i] - C_p + 120\log_{10}(\|\boldsymbol{x}_0 - \boldsymbol{x}_i\|)\right\|^2$. The above problem is also solved using gradient descent to iteratively find the optimal $\boldsymbol{x}_0$. We also compared with anchor-based solution, where four anchors are placed at the four corners of a plane with a depth of half of the maximum depth. The problem is formulated the same as the baseline model, i.e., the anchor-based model is equivalent to the robot-based solution with four waypoints.

In the simulation model, we consider the robot moves on the ground following a predefined trajectory, as shown in Fig. 2. There are 10 waypoints aligned along two rows. The first waypoint's location is $(-0.25, -0.10, 0)$m, and the last waypoint's location is $(-0.35, 0.10, 0)$m. The mutual interval between two waypoints in a row is 0.1 m. The sensor is uniformly distributed in an area with $x \in [0, 0.5]$m, $y \in [0, 0.5]$m, and $z \in [-0.6, -0.1]$m. We do not consider the scenario where the sensor's depth is smaller than 0.1 m. When the depth is small, the received signal is strong and the location can be easily estimated. The attenuation coefficient is randomly sampled from the 2020 data. The simulation parameters are summarized in Table 1.

In the simulation, we consider the following four scenarios: (1) the previous hourly attenuation coefficient and the standard deviation is available; (2) the previous daily attenuation coefficient and the standard deviation are available; (3) an initial inaccurate estimation of the attenuation coefficient and its standard deviation during a year is available; and (4) the attenuation coefficient is not considered in the model, i.e., the baseline model. In Fig. 6, Fig. 7, and Fig. 8, these scenarios are denoted by "Hour", "Day", "Unknown α", and "Baseline". The squared localization error is defined as $\|\tilde{\boldsymbol{x}}_0 - \boldsymbol{x}_0\|^2$, where $\tilde{\boldsymbol{x}}_0$ is the estimated localization. The root-mean-square error (RMSE) is defined as $\sqrt{\sum_i^{N_{sim}} \|\tilde{\boldsymbol{x}}_0^i - \boldsymbol{x}_0^i\|^2 / N_{sim}}$, where N_{sim} the

Table 1: Simulation Parameters

Symbol	Value	Symbol	Value
C_m	1×10^{-10}	μ	$4\pi\times10^{-7}$
ϵ	8.854×10^{-12}	P_t	0.01 W
σ_n	5	$\boldsymbol{x}_0^1$	(0.1,0.1,-0.1)m

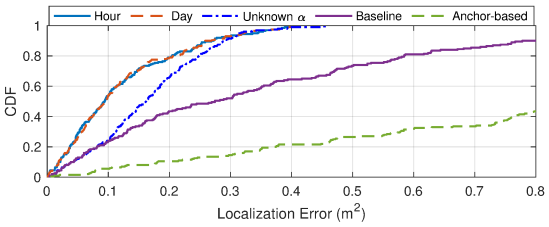

Fig. 6: CDF of localization error with $z_{min} = -0.6$m.

simulation number. Note that, in the estimation, we consider the sensors can be anywhere underground, i.e., there is no constraint in the x and y directions. Moreover, at each waypoint, the robot collects 10 samples and uses the mean value as the received power to reduce the noise impact.

In Fig. 6, we consider a large area with the depth $z_{min} = -0.6$ m. We run $N_{sim} = 200$ simulations and randomly select the attenuation coefficient from the second one to the last one. The standard deviation of the "unknown α" case is set as 1. This allows the EM algorithm to iterate in a large range to obtain the optimal expectation value. The maximum iteration number N_{step} is set as 10. For the "Hour" and "Day" cases, the standard deviations are small, as shown in Fig. 5. Thus, the expectation computation converges fast, and we use $N_{step} = 2$ for these two cases. Last, for the "Baseline" model, since there is no iteration for α, N_{step} is 1. However, the "Baseline" model has iterative computation for the optimal localization for the gradient descent optimization, which is accomplished using the standard MATLAB optimization function fminunc. As shown in the figure, with prior information about α, the "Hour" and "Day" achieve the lowest error and there is no obvious difference between their performances. This is due to the fact that soil dynamics are relatively slow processes. There is no significant difference between the hourly change and the daily change. Also, without knowledge of α, we use a rough estimation of 1.43 and this number can be different, which results in a similar performance. The performance of the "Unknown α" is slightly worse than the previous two cases due to the lack of attenuation coefficient information. However, this is a more practical case for most underground applications. Last, if the attenuation coefficient is not considered, only 60% of the simulations can get a squared localization error smaller than 0.4, while it is nearly 100% for the previous three cases. The anchor-based solution performs much worse because it only has 4 anchor nodes. Compared with the 10 waypoints, the anchor number is small and the anchors cannot collect sufficient spacial information.

In Fig. 7, we consider a smaller area with $z_{min} = -0.4$ m. Since the underground battery-free sensors have a shorter distance to the aboveground robot, the received power is stronger. As shown in the figure, the squared localization error is smaller for all the cases compared with that in Fig. 6. The RMSE for both Fig. 6 and Fig. 7 is shown in Fig. 8. With the attenuation coefficient information, the RMSE is around 0.31 m, while for unknown α it is around 0.36 m. Without considering the dynamics, the RMSE is higher than 0.5 m.

V. CONCLUSION

Localizing underground sensors using a single robot finds many applications for the Internet of Things in agriculture. In this letter, a single robot moves along a predefined trajectory to collect Received Signal Strength data at multiple waypoints to emulate an antenna array. The soil conductivity and permittivity are dynamic parameters that can affect the accuracy of underground localization. In this letter, the expectation-maximization algorithm is used by considering the soil attenuation coefficient as a latent variable. Numerical simulations have shown that the proposed localization algorithm can achieve significant gain compared with a baseline model which does not consider dynamic soil parameters.

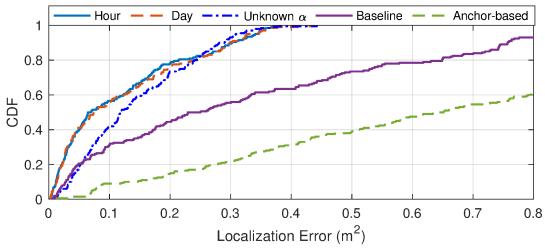

Fig. 7: CDF of localization error with $z_{min} = -0.4$m.

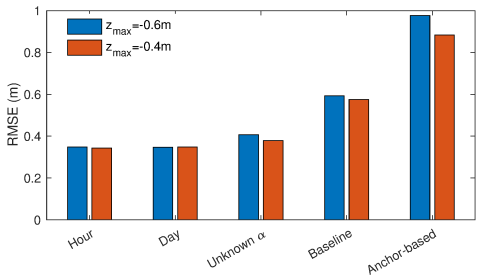

Fig. 8: Root-mean-square error with $z_{min} = -0.6$m and $z_{min} = -0.4$m.

REFERENCES

[1] B. Zhou, V. S. S. L. Karanam, and M. C. Vuran, "Impacts of soil and antenna characteristics on lora in internet of underground things," in *2021 IEEE Global Communications Conference (GLOBECOM)*. IEEE, 2021, pp. 1–6.

[2] G. Di Renzone, S. Parrino, G. Peruzzi, A. Pozzebon, and D. Bertoni, "Lorawan underground to aboveground data transmission performances for different soil compositions," *IEEE Transactions on Instrumentation and Measurement*, vol. 70, pp. 1–13, 2021.

[3] H. Yin, Y. Cao, B. Marelli, X. Zeng, A. J. Mason, and C. Cao, "Soil sensors and plant wearables for smart and precision agriculture," *Advanced Materials*, vol. 33, no. 20, p. 2007764, 2021.

[4] H. Guo and A. A. Ofori, "The internet of things in extreme environments using low-power long-range near field communication," *IEEE Internet of Things Magazine*, vol. 4, no. 1, pp. 34–38, 2021.

[5] Z. Sun and I. F. Akyildiz, "Magnetic induction communications for wireless underground sensor networks," *IEEE transactions on antennas and propagation*, vol. 58, no. 7, pp. 2426–2435, 2010.

[6] R. Zhao, P. Wang, Y. Ma, P. Zhang, H. H. Liu, X. Lin, X. Zhang, C. Xu, and M. Zhang, "Nfc+ breaking nfc networking limits through resonance engineering," in *Proceedings of the Annual conference of the ACM Special Interest Group on Data Communication on the applications, technologies, architectures, and protocols for computer communication*, 2020, pp. 694–707.

[7] X. Zhang, A. Andreyev, C. Zumpf, M. C. Negri, S. Guha, and M. Ghosh, "Thoreau: A subterranean wireless sensing network for agriculture and the environment," in *2017 IEEE conference on computer communications workshops (INFOCOM WKSHPS)*. IEEE, 2017, pp. 78–84.

[8] ——, "Thoreau: A fully-buried wireless underground sensor network in an urban environment," in *2019 11th International Conference on Communication Systems & Networks (COMSNETS)*. IEEE, 2019, pp. 239–250.

[9] W. Yuan, N. Wu, B. Etzlinger, Y. Li, C. Yan, and L. Hanzo, "Expectation–maximization-based passive localization relying on asynchronous receivers: Centralized versus distributed implementations," *IEEE Transactions on Communications*, vol. 67, no. 1, pp. 668–681, 2018.

[10] P. Bromiley, "Products and convolutions of gaussian probability density functions," *Tina-Vision Memo*, vol. 3, no. 4, p. 1, 2003.

[11] S. Boyd, S. P. Boyd, and L. Vandenberghe, *Convex optimization*. Cambridge university press, 2004.